

EXPERIMENTAL VALIDATION OF TOW-STEERED COMPOSITE WINGS FOR AEROELASTIC DESIGN

O.Stodieck¹, G.Francois¹, D.Heathcote², E. Zypeloudis¹, B.C.Kim¹, A.T.Rhead²,
D.Cleaver², J.E.Cooper¹

¹ Department of Aerospace Engineering,
University of Bristol, Bristol, UK
j.e.cooper@bristol.ac.uk

² Department of Mechanical Engineering,
University of Bath, Bath, UK
A.T.Rhead@bath.ac.uk

Keywords: aeroelastic tailoring, tow-steering, aeroelastic optimisation

Abstract: A numerical and experimental investigation is described considering the design, manufacture and test of tow-steered composite wind tunnel wings. The generic construction of each wing consisted of a rectangular flat plate with foam aerofoil surfaces. Tow-steered composite layers of the wings were manufactured using two different techniques: Continuous Tow-Shearing and Discrete Stiffness Tailoring. Finite Element models of the wings were optimised in order to determine the tow-steered composite layer orientations, as well as uni-directional composite orientations, that reduced the maximum strains due to equivalent “manoeuvre” and “gust” loads (at a tunnel speed of 20 m/s). A series of static and dynamic, wind-on and wind-off tests were performed to validate the numerical modelling capability and to illustrate the capabilities of tow-steering technologies.

1 INTRODUCTION

There is an increasing drive to develop aircraft designs that are more efficient and environmentally friendly, as defined by the likes of the EU FlightPath 2050 initiative. One approach to achieve this is to make much greater use of composite materials in the aircraft structure in order to exploit the beneficial strength – weight characteristics; aircraft such as the A350 and B787 contain a large percentage of composites. Through exploitation of the anisotropic characteristics of composite materials it is possible to optimise the bending/torsion coupling characteristics of aircraft wings in a passive manner, an approach referred to as aeroelastic tailoring [1,2].

Significant work has been done in the area of aeroelastic tailoring of composite wing structures since the early 1980s where the concept was first demonstrated on the X-29 experimental aircraft; a washout effect (wing up-bend coupled to nose-down twist) was used to increase the divergence speed of the forward-swept wing [1,2]. Many other numerical studies have used aeroelastic tailoring with the objectives of: weight and drag reduction, improved gust response and optimum flutter behaviour, and various combinations of these objectives, e.g. [3]. All of these studies involve modifying the stiffness of the wing and the passive elastic coupling between wing bending and torsional deformations, so as to improve the static and dynamic wing

behaviours in different airflows. With composite wing structures, the fibre angles and layup sequences can be tailored to optimise the stiffness and bending-torsion coupling over the span of the wing. To become feasible, these concepts rely on a multidisciplinary design optimisation (MDO) approach; however, the potential benefits of aeroelastic tailoring may currently be diminished due to the limited design space available with standard unidirectional (UD) laminates, which tend to be homogenised orthotropic $0^\circ/\pm 45^\circ/90^\circ$ ply laminates. In order to change the stiffness or bending-torsion coupling of such a UD laminate, either the whole ply stack has to be rotated relative to the part, or plies of specific fibre orientations have to be added or dropped.

Over the last twenty years, so-called “tow-steering” techniques have been developed to manufacture laminates with variable angle tow (VAT) plies (also called variable-stiffness plies), including automatic fibre placement (AFP), tailored fibre placement (TFP), continuous tow shearing (CTS) [4-7] and Discrete Stiffness Tailoring [8]. The fibres in these plies are locally unidirectional through the thickness of the ply (as opposed to multi-axial, woven or braided materials), but they follow predefined curvilinear paths within the plane of each ply, such that the fibre angles and ply stiffness vary continuously. It has been demonstrated that the curvilinear fibre paths can be optimised to increase the structural performance of VAT laminates beyond that of equivalent UD laminates for a range of applications. However, there has been very little work published on the use of VAT composites for aeroelastic tailoring. Numerical work at the University of Bristol [9-11] has shown that optimal stiffness tailoring of composite wings (See Fig.1(a)) has the potential to significantly improve aircraft performance through the exploitation of aeroelastic deflections to: maintain optimal aerodynamic shape throughout the flight envelope, alleviate gust loads and extend flutter boundaries.

From the manufacturing point of view, novel stiffness tailoring techniques, Continuous Tow Shearing (CTS, Fig.1 (b)) [4-7] and Discrete Stiffness Tailoring (DST) [8], developed at the Universities of Bristol and Bath respectively, have reached sufficient maturity to experimentally demonstrate such concepts, having already demonstrated weight reduction through increased buckling capacity (See Fig. 1 (c)). However, there has been no experimental demonstration of tow steered methodologies for aeroelastic tailoring.

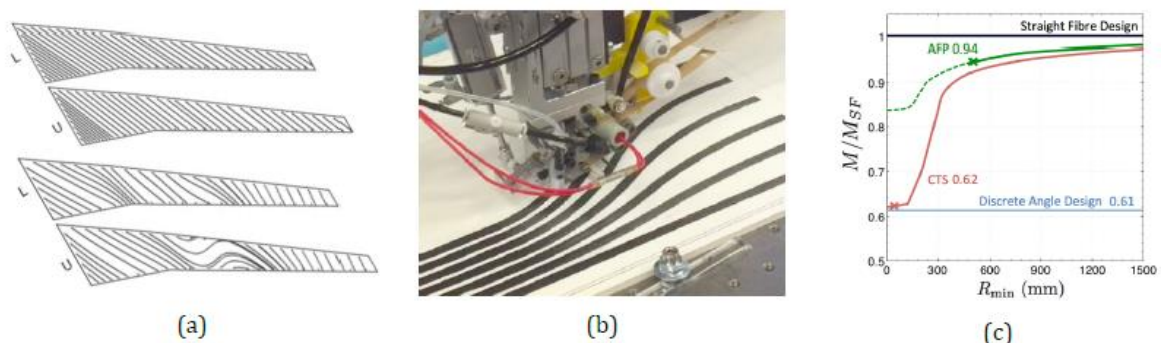


Figure. 1 a. Upper and lower surfaces for unidirectional and tow steered optimal flutter solutions (the tow steered solution resulted in 17% reduction in wing weight [11]), b. Continuous Tow Shearing machine [5], c. Panel masses (normalised against straight fibre mass M_{SF}) versus radius of curvature constraint for various stiffness tailoring techniques for optimum buckling capacity. Crosses denote limits of manufacturability [6].

This paper reports on a study to experimentally validate advanced multi-physics modelling for stiffness tailored aeroelastic structures, and demonstrate the design and manufacture of stiffness

tailored composite wings for wind tunnel testing. These goals were achieved by completing the following:

- Design of stiffness tailored wind tunnel sized wings using the multi-physics modelling approaches developed at the University of Bristol [9-11]
- Manufacture and testing of stiffness tailored wind tunnel sized wings based on several different tow-steering techniques and evaluation of aeroelastic performance

Two manufacturing techniques are considered:

Continuous Tow Shearing (CTS) continuously steers individual fibres within each tow by continuously shearing the tow tapes with high accuracy and without defects. Its minimum steering radius (approx. 50 mm) is an order of magnitude less than that of commercial AFP machines, allowing for manufacturing small-sized tow steered wing models for wind tunnel testing. Flat tow steered preforms were produced using the CTS machine on a flat substrate and transferred to flat and aerofoil shaped curved moulds for autoclave curing.

Discrete Stiffness Tailoring (DST) places a series of straight fibre prepreg strips with discrete angle changes to approximate the designed fibre paths across the wing span. This technique allows for single axis ATL deposition and thus high productivity in manufacturing tow steered composites.

The wind tunnel wing demonstrators were designed, manufactured and tested with quasi-isotropic (“black-metal”), unidirectional and tow-steered lay-ups. Flat tow steered plates for optimum stiffness distribution were designed to an aeroelastic goal (minimum material strains for given aeroelastic static and dynamic loads) (e.g. washout for increasing aerodynamic pressure and/or gust loads alleviation). Foam aerodynamic surfaces were added to provide an aerodynamic shape. The flat panel models focused on the validation of the optimisation method by minimising the complexity in manufacturing.

A range of static and dynamic tests was performed both in the laboratory and also in the wind tunnel at both universities. The results were then compared with the numerical predictions.

Static and Dynamic Bench (Wind-off) Testing

Static tests were performed to measure the stiffness characteristics, bending/torsion coupling and the flexural axis position [12]. Dynamic tests were undertaken to determine the modal parameters (natural frequencies, damping ratios and mode shapes).

Wind Tunnel Testing

Static aeroelastic tests were performed to measure the deflections, wing root lift and pitching moment due to increasing dynamic pressure and root angle of attack.

2 WING DESIGN AND AEROELASTIC OPTIMISATION

2.1 Wing Model Description

The test specimens were made from flat rectangular composite plates of 0.5 m span and 0.1 m chord, covered with aerofoil-shaped foam fairings (NACA0012) of 0.15 m chord, as shown in Fig. 5(a). The plate was made using 10 plies of a carbon/epoxy prepreg (MTM49-3/T800, Solvay, US) laid up symmetrically, with the mechanical properties listed in Table 1.

Only the fibre orientations of the outer 4 plies of each laminate were taken as design variables, since these plies have the largest impact on the wing bending and torsion stiffness. Finite element models (FEMs) of the specimens were developed using MSC Nastran [10] with the plates modelled using 2D shell elements, coupled with doublet-lattice method (DLM) aerodynamics for the static and dynamic aeroelastic loads predictions. The foam fairings were not modelled, since the static bending test of the wing with foam fairings showed that their contribution to the bending stiffness was negligible.

2.2 Optimisation approach

The following four different specimens were designed, manufactured and tested:

- (1) Straight-fibre laminate with bend-twist coupling
- (2) CTS laminate with bend-twist coupling
- (3) DST laminate with bend-twist coupling
- (4) Straight-fibre laminate without coupling

Specimens 1-3 were designed to reduce the maximum strains due to “manoeuvre” and “gust” loads (at 20 m/s). Since the number of plies was constant (no ply drops), lower strains were indicative of a more efficient design. Specimen 4 was not optimised and used for FE model validation purposes only. The optimisation problem may be stated as

$$\begin{aligned} & \text{Min. (Max}|\varepsilon|) \\ & \text{s.t. } \xi \geq 0 ; \\ & -45^\circ \leq \theta \leq 45^\circ \end{aligned} \quad (1)$$

where ε is the vector of principal strains measured at all elements for 2 different load cases: 1) a static 6N lift trim case at 20 m/s, 2) dynamic forced tip deflection case with zero angle of attack at the wing root, at 20 m/s. Flutter and divergence constraints were implemented by constraining the damping ratio ξ to be positive in the velocity range up to 30 m/s. Formulations for the static and aeroelastic analyses are described in reference [9].

The optimisation variables θ correspond to the fibre orientations in the 4 outer plies. As the laminates were symmetric, only 2 variables were used for specimen (1). For specimen (2), fibre orientations were defined at 10 spanwise control points in each ply, with interpolation of the fibre angle variation using quadratic B-splines [9], resulting in a total of 20 variables. A gradient based algorithm (GCMMA [12]) was used to optimise specimens (1) and (2). Post-optimisation, the constant fibre angle sections of specimen (3) were approximated from the continuous variations of specimen (2).

E_1 (GPa)	163	ν_{12}	0.28
E_2 (GPa)	6.8	t (cured ply thickness, mm)	0.14
G12 (GPa)	3.4	ρ (kg/m ³)	1600

Table 1. Material properties (MTM49-3/T800)

2.3 Optimised wing designs and aeroelastic performance

The designed fibre angle variations for specimens (1) to (3) are shown in Table 2 and Fig. 2. The $[0/0/0/45/-45]_s$ laminate for specimen (4) was chosen to minimise the bend-twist coupling of the wing, whilst also maximising the bending stiffness.

The peak strains along the wing span for the static load case are plotted in Fig. 2 (a). The optimised variable stiffness specimen design (2) generated the lowest peak strains ($224\mu\epsilon$) at the wing root, which corresponds to a 19% strain reduction compared to the optimised straight fibre laminate specimen (1) ($276\mu\epsilon$). The strain reduction was achieved by increasing the bending stiffness at the wing root and by inducing favourable bend-twist coupling on the outer wing, with the wing twisting to reduce the outboard angle of attack (washout). To achieve the same total amount of lift, the wing root angle of attack was slightly increased for specimen (2) (3.57°) compared to specimen (1) (3.48°).

Fig. 2 (b) shows the peak principal strains along the wing span for the dynamic load case, where the variable stiffness designs result in higher outboard strains than the straight fibre laminates, due to the increased wing flexibility. The peak dynamic strain for specimen (2) ($226\mu\epsilon$ at $y=0.155\text{m}$) was approximately equal to the peak static case strain, indicating that the design of specimen (2) was driven by both the static and dynamic load cases. The significantly higher peak dynamic strain for specimen (3) ($300\mu\epsilon$ at $y=0.295\text{m}$), is a sign that the DST specimen design derived from the CTS specimen (2) was probably sub-optimal. Indeed, this discrepancy may be reduced by optimising the layup for specimen (3) directly using a piece-wise constant fibre angle variation (approach now used in follow-on work).


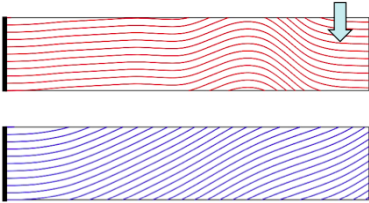
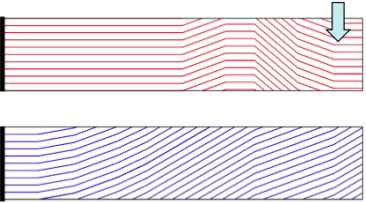
Straight Fibre	CTS (Continuous Tow Shearing)	DST (Discrete Stiffness Tailoring)
$[0/30/0/45/-45]_s$	$[\theta_1/\theta_2/0/45/-45]_s$	$[\theta_1/\theta_2/0/45/-45]_s$
		

Table 2. Fibre angle variations in the tailored outer plies on specimens (1)-(3), where ply 1 is the outermost ply, the wing root is on the left and the blue arrow indicates the air flow direction over the wing.

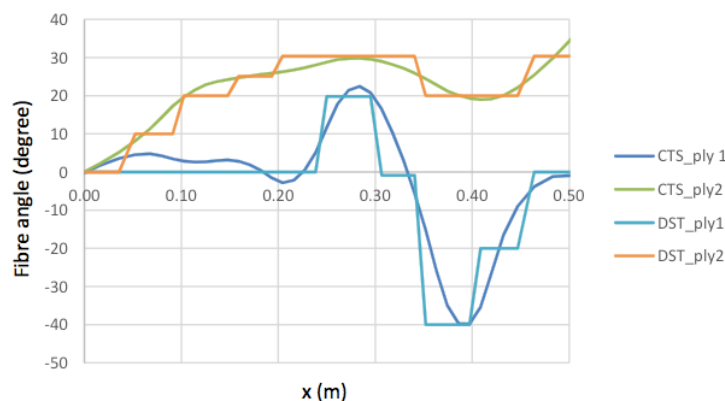


Figure 2. Fibre angle variations for the CTS and DST designs.

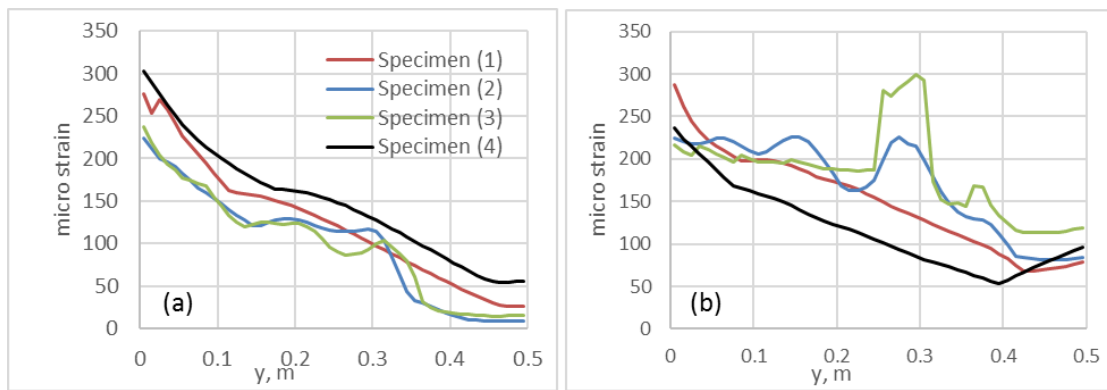


Figure 3. Maximum absolute principal strain distribution along the wing span (aligned with the y-direction) for the (a) static 6N lift trim case at 20m/s, (b) dynamic forced tip deflection case with zero angle of attack at the wing root, at 20 m/s.

3 MANUFACTURING METHODS

3.1 Continuous Tow Shearing (CTS)

The CTS process can steer individual fibres within each tow by continuously shearing the tow tapes with high accuracy and without defects [4-5]. Its minimum steering radius (approx. 50 mm) is an order of magnitude less than that of commercial AFP machines, allowing for the manufacturing small-sized tow steered wing models for wind tunnel testing. One of the major advantages of this continuous shearing process is that the material width does not affect the steering radius. Since the maximum fibre steering angle required for the optimised design was only 40° , a 100 mm wide standard carbon/epoxy prepreg tape (MTM49-3/T800) was used for the wide tape shearing CTS head [6,7]. Fig. 4 (a) shows the CTS prototype head laying up the top ply of the tow-steered wing. In order to reduce the shear stiffness of the prepreg tape, a heater attached within the head increased the temperature to $50\text{-}60^\circ\text{C}$. The lay-up speed was 12 mm/s. Multiple tapes with the same fibre path were laid next to each other along the tape width direction, and then cut into rectangular sheets with the dimensions of the flat wing. The prepreg sheets with the θ_1 and θ_2 angle variations (See Fig. 2) were prepared, and stacked manually with straight fibre prepreg sheets to achieve the $[\theta_1/\theta_2/0/45/-45]_s$ stacking sequence. The stacked preform was cured at 125°C using the vacuum bag moulding process in the autoclave (2 hours at 7 bars), and a rigid aluminium plate and a flexible 3 mm thick silicone rubber sheet were used at bottom and top to form a smooth outer surfaces. Fig.4 (b) shows the bottom surface of the cured flat wing. Although the minimum steering radius was only 60 mm, there was no significant fibre wrinkle or resin pocket, and the fibre trajectory followed the reference path (in red) with high lay-up accuracy, which can never be achieved by any existing modern AFP or ATL machine.

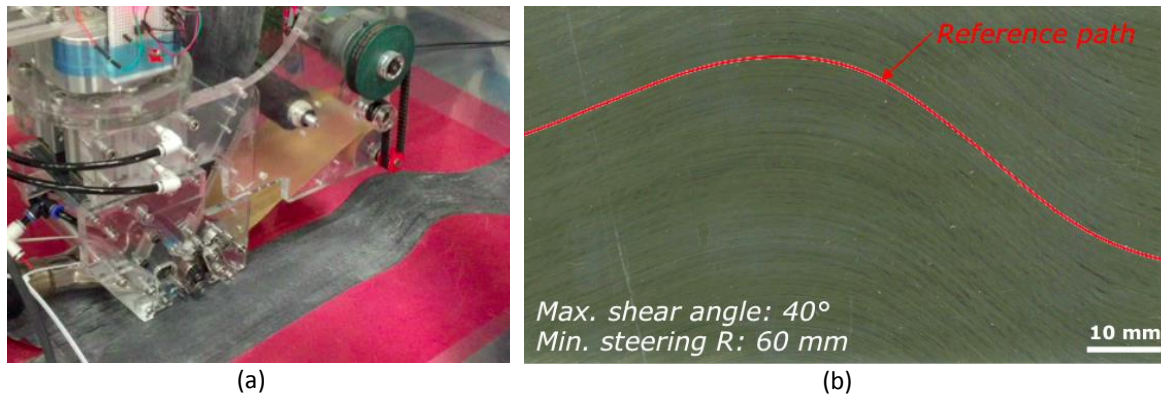


Figure 4. CTS prototype head and the quality of the fibre steering: (a) CTS head laying up a 100 mm wide prepreg tape; (b) the bottom surface of the cured laminate.

3.2 Discrete Stiffness Tailoring (DST)

To enable comparison of fibre steering effectiveness, the DST panel was constructed using the same material (MTM49-3/T800) as the CTS and straight fibre (UD with and without bend twist) wing panels. Layup of the plies was performed by hand, before curing. The cure cycle employed for the DST panel was identical to that used at the University of Bristol for the CTS and UD panels, to ensure consistency.

As for the CTS panel, the DST panel was comprised of ten plies with a symmetric layup; the outer four (two upper and two lower surface) plies of the stacking sequence having been optimised to reduce maximum principal strain (as described in section 1). Manufacture of the laminated composite test specimens using Discrete Stiffness Tailoring (DST) required the continuous optimised fibre path derived in Section 1 to be approximated by a piecewise linear function with 10 discrete fibre angles. The discrete fibre angles were obtained by considering the mean angles of the optimised fibre angle variation following a quadratic B-spline in ten 50 mm wide sections along the panel length, as shown in Table 2. This allowed the upper two fibre steered plies of the test panels to each be constructed from 10 sections across the span with each section having its own constant fibre angle. Sectioning of the upper plies creates ‘seams’ where discrete changes in fibre angle occur. In order to provide adequate shear stress transfer at these locations, discontinuities in the θ_1 and θ_2 plies were offset by 10 mm.

3.3 Wind tunnel demonstrator manufacturing

Fig. 5 (a) shows the schematic of the wing demonstrator, which consists of a flat fibre-steered composite laminate and polystyrene foam fairings. Three different flat composite laminates with bend-twist coupling effect, which are listed in Table 1, were manufactured in addition to a straight fibre design $[0/0/0/45/-45]_s$ without bend-twist coupling effect as a reference.

The root of the flat wing was extended by 50 mm, and glass fibre composite tabs were bonded to prevent damage at clamping. Before attaching the foam fairings, three rosette strain gauges were attached on the top and bottom surfaces of the flat wing as shown in Fig. 5 (b). The cross-sectional shape of the foam fairing followed the NACA0012 aerofoil geometry. Each foam fairing was covered by a thin plastic film with an overhang covering the gap between adjacent fairings.

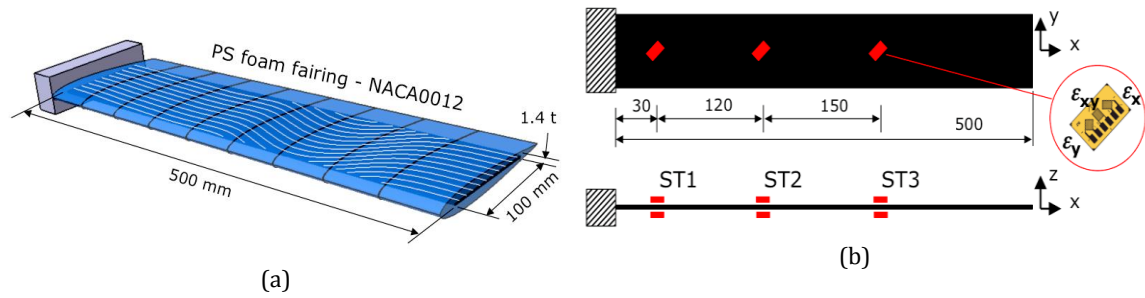


Figure 5. Schematics of the wing demonstrator. (a) overall dimensions, (b) locations of the strain gauges.

4 STATIC WIND TUNNEL TEST RESULTS

Static wind-off and wind-on tests were performed for each plate. For each test, tri-axial strains were recorded at three different locations across the span, as shown in Fig. 5 (b), of the top and bottom side of each plate alongside the root forces/moments and tip region deflections. The strains were measured using 350Ω rosettes with strain gauges in the 0° , 45° and 90° direction. Forces and moments at the root were recorded using a 6-axis load cell.

At the University of Bristol, all static tests were carried out in the low turbulence wind tunnel. The plates were placed horizontally in the tunnel as shown by Fig. 6. A 3D Dantec Q400 Digital Image Correlation (DIC) system was used to measure wing deflections of the tip region (from the tip to 200 mm inboard). The two DIC cameras were placed outside the wind tunnel looking towards the underside of the plates through an acrylic wall.

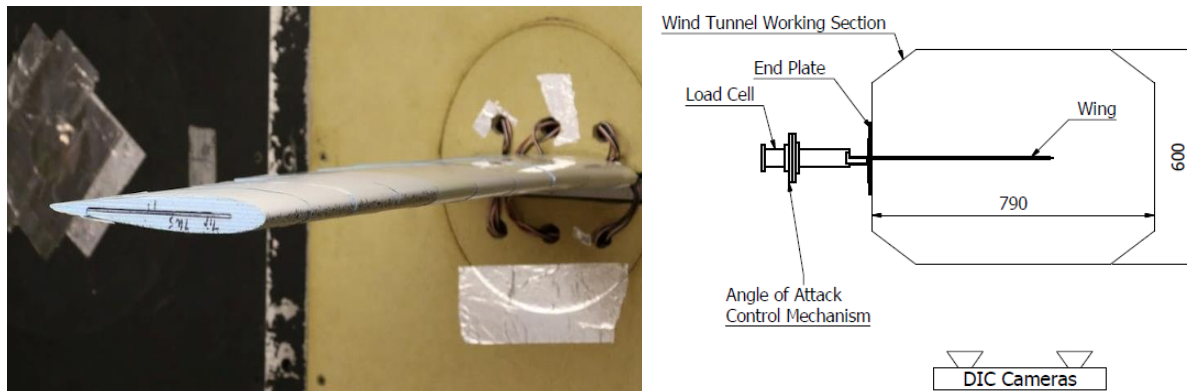


Figure 6. Wind tunnel test set-up.

4.1 Wind-off test

Two static wind-off tests were considered. The specimens were first tested by applying incrementally increasing shear loads at the wing tip (normal to the plane of the plate). Shear forces were applied at the plate half-chord and also at offset locations, which induced bending and torsion deflections along the span. At UoB, the first static wind-off test consisted of applying three successive static weights (85, 125 and 165g) symmetrically by the mid-chord line at the tip of the plates so that the plate with no bend-twist coupling experienced only bending loads. The second static wind-off test consisted in applying three successive static weights (85, 125 and 155g) at the tip of the plates but with more weights applied at the tip

leading edge of the plate so that bending and torque loads were created (20, 40 and 50g extra weights applied at the tip leading edge than at the tip trailing edge). The test was carried out for the three flat composite plates with and without the foam fairings. The test was repeated at least three times for each plate. The strains, loads at the root and deflections were simultaneously recorded for every test.

A sub-set of the measured wing deflections and strains are compared to the finite element analysis predictions, as shown in Figs. 7 and 8. Experimental uncertainty in the rigidity of the wing root boundary conditions and in the load input locations are likely to have had a significant effect on the measured wing tip deflections and twist. However, overall, the strain and tip deflection trends correlate well, validating the stiffness modelling and manufacturing accuracy of the wing. By performing these tests with and without foam fairings, it was also verified that the wing stiffness was not significantly affected by the stiffness of the fairings. Note that the error is very small on all measurements, resulting in no error bars being shown on the plots.

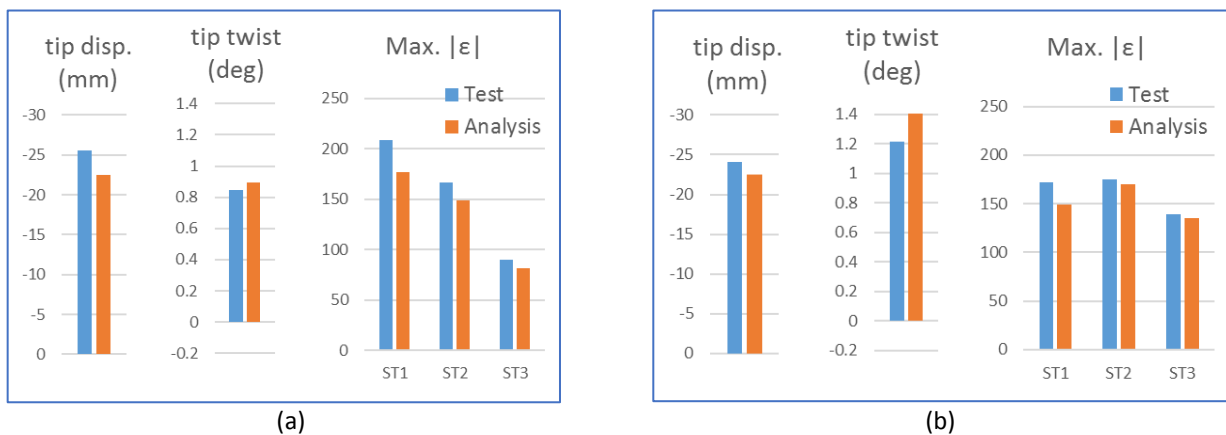


Figure 7. Test and FEM analysis results for a combined -1.5N shear force and -25Nmm torque test case: (a) the optimised straight fibre (UoB) specimen (1); (b) the CTS specimen (2).

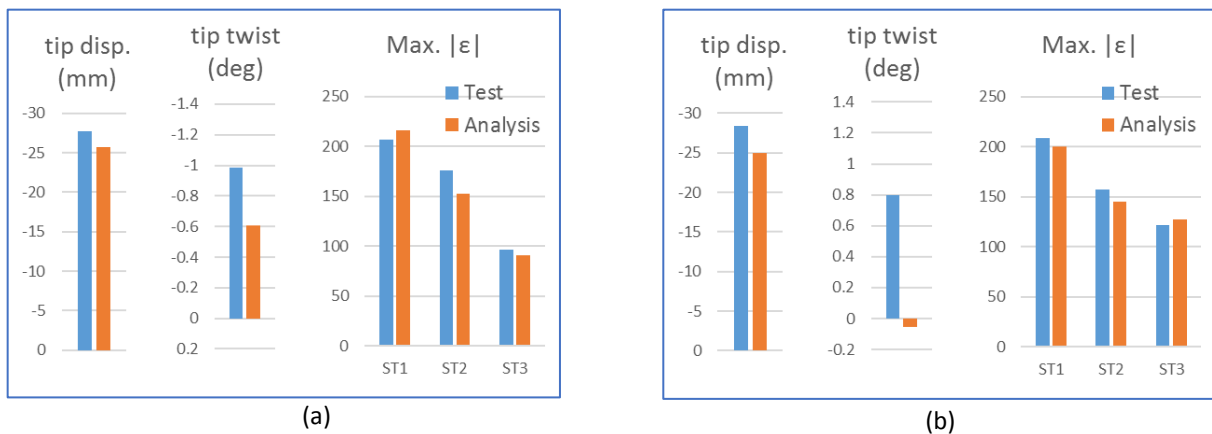


Figure 8. Test and FEM analysis results for a combined -1.8N shear force and -91Nmm torque test case: (a) the optimised straight fibre (UoBath) specimen (1); (b) the DST specimen (3).

4.2 Wind-on test

The static wind-on test consisted of measuring the wing response under aerodynamic loading by varying the angle of attack and airspeed. The test was performed for two angles of attack (1.6 and 3.6°) and three airspeeds (10, 15 and 20 m/s) were used. The test was performed on the three flat composite plates with the foam fairings. The test was repeated three times for each

plate. Simultaneous recording of the strains, loads at the root and deflections was performed for every test. Fig. 9 shows the bend-twist behaviour of the wings with the stacking sequences of $[0/0/0/45/-45]_s$ and $[\theta_1/\theta_2/0/45/-45]_s$ at the angle of attack of 3.6° , as an example.

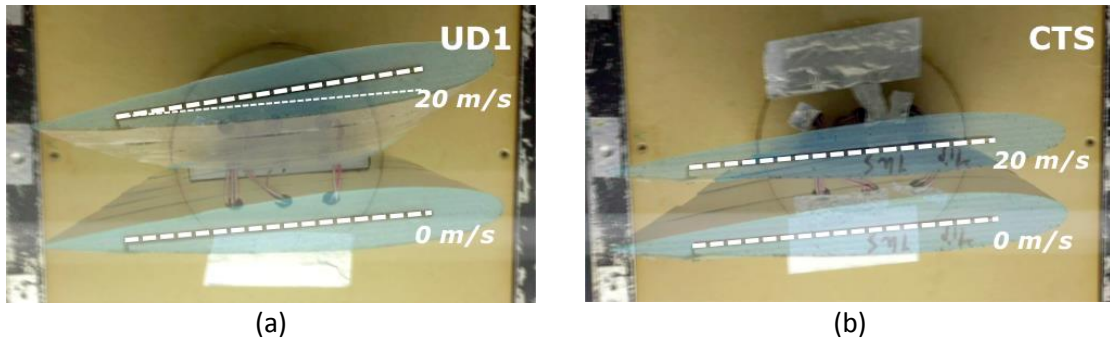


Figure 9. Bend-twist behaviours of the wings with different fibre orientations (3.6° AoA): (a) $[0/0/0/45/-45]_s$ without bend-twist coupling, (b) $[\theta_1/\theta_2/0/45/-45]_s$ with bend-twist coupling.

A sub-set of the measured wing deflections and strains are compared to the FEM predictions in Figs. 10 and 11. Overall, the strain and tip deflection trends correlate well, validating the aeroelastic modelling of the wing.

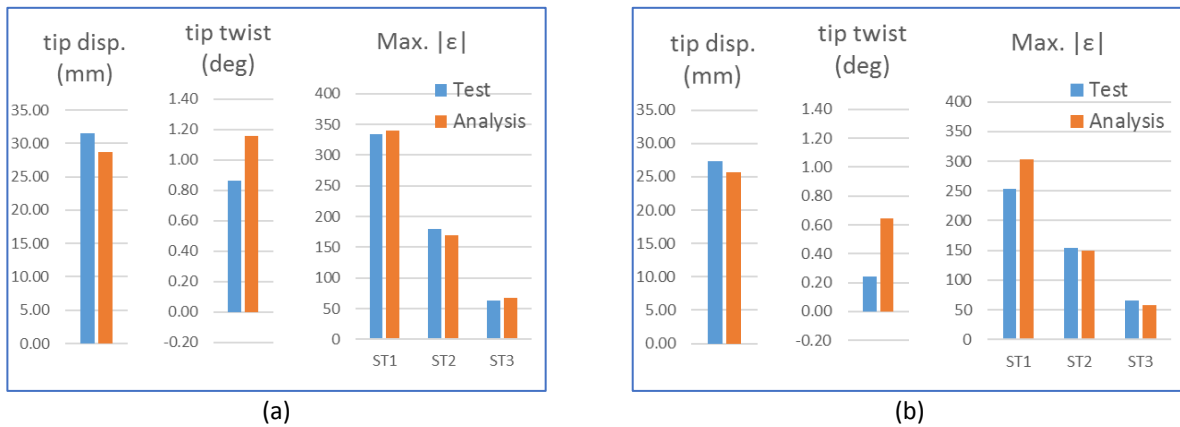


Figure 10. Test and FEM analysis results for a wing root angle of attack of 3.6° and flow velocity of 20 m/s (horizontal wing test setup at UoB): (a) the optimised straight fibre (UoB) specimen; (b) the CTS specimen.

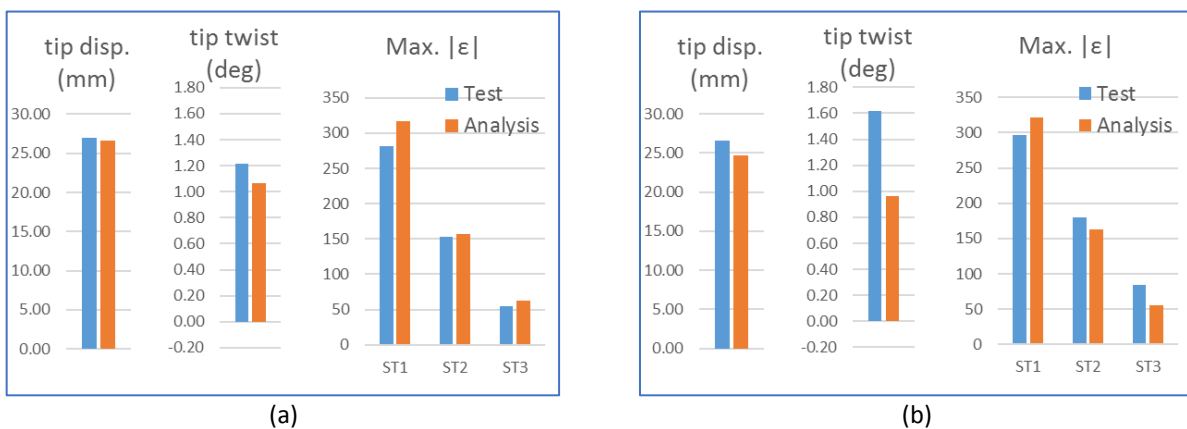


Figure 11. Test and FEM analysis results for a wing root angle of attack of 3.6° and flow velocity of 20 m/s (vertical wing test setup at UoBa): (a) the optimised straight fibre (UoBa) specimen; (b) the DST specimen.

Aeroelastic measurements of the DST and UD with bend-twist coupling panels were undertaken in the University of Bath wind tunnel, as shown in Fig. 12. For the University of Bristol experiments, the panels were assessed both with and without the addition of ten foam fairing sections of a NACA0012 profile with a chord length, $c = 150$ mm, that formed an aerofoil across the full panel. Due to differences in the experimental set up between the Universities of Bath and Bristol (wing suspended vertically and horizontally respectively), corresponding results for lift coefficient were expected to differ slightly. The horizontally suspended panels at the University of Bristol had an initially deformed shape, meaning less lift was produced.

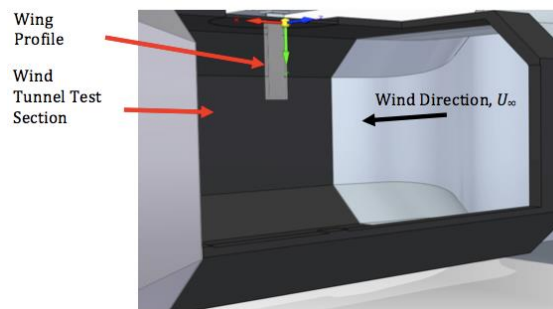


Figure. 12 Schematic of the University of Bath's large wind tunnel with the wing shown *in-situ*.

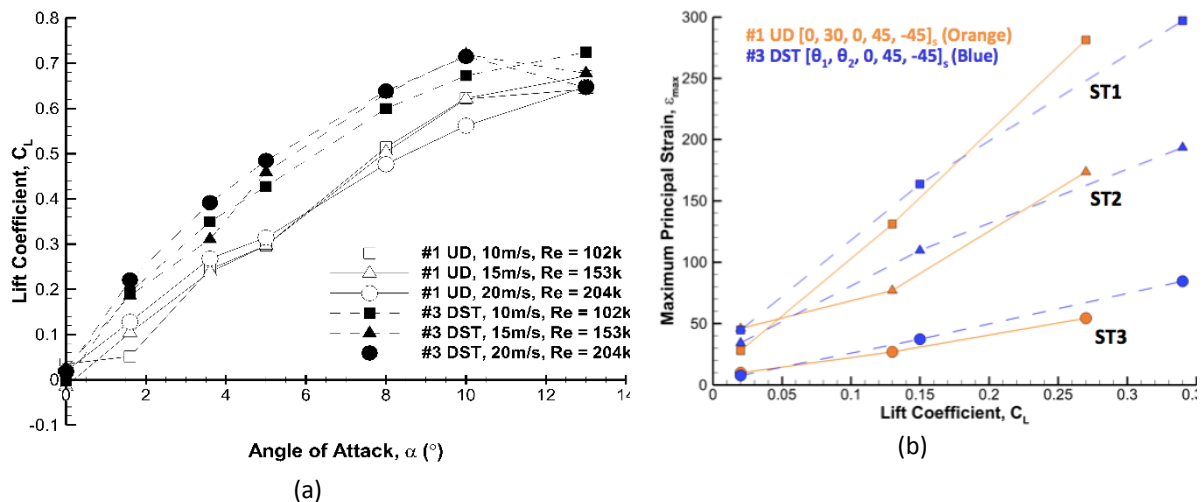


Figure 13. (a) Lift coefficient vs. angle of attack for UD and DST specimens; (b) Maximum principal strain vs. Lift coefficient for UD and DST specimens for strain gauge rosettes located at ST1-ST3.

Tests were completed at the same testing conditions as at the University of Bristol ($U_\infty = 10, 15$ and 20 m/s corresponding to Reynolds numbers, $Re = 102,000, 153,000$ and $204,000$ respectively). Multi-axis root load was measured for angles of attack in the range $0^\circ \leq \alpha \leq 13^\circ$, while full field displacement and surface strain measurements at discrete locations were conducted at $0, 1.6$ and 3.6° . A schematic of the test set up is presented in Fig. 12. The wind tunnel test section was of dimensions 2.13×1.51 m, with a turbulence intensity measured to be 0.5% at $U_\infty = 20$ m/s.

Fig. 13 (a) plots lift coefficient, C_L , against angle of attack, α for the University of Bath aerofoil section tests and the results indicate that the DST panel creates a higher lift coefficient for the same angle of attack when compared to the UD panel. Thus, in order to accurately compare the strain measured for different aerodynamic conditions on each wing, Fig.13 (b) plots C_L , against maximum principal strain, ϵ_{max} , averaged between the upper and

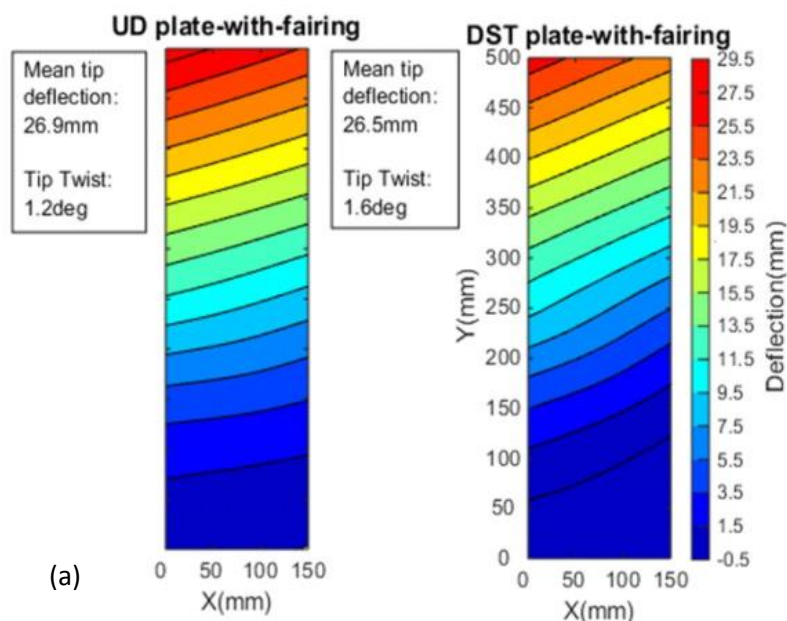
lower surfaces for the two panels. From this, a trend between maximum principal strain and lift coefficient could be extracted, see Table 3. It can be noted that although the DST produces a higher lift coefficient, the maximum principal strain produced is extremely similar to that for the UD panel at the same angle of attack. As such, there is a reduction in the $\epsilon_{max}-C_L$ gradient, indicating a reduction in strain for the DST panel if the lift coefficient values were matched. The $\epsilon_{max}-C_L$ gradient is reduced by 14%, when comparing the UD to DST panel, indicating aeroelastic stiffness tailoring using DST is a viable technique in reducing maximum principal strain.

Location	$\epsilon_{max} - C_L$ gradients		
	ST1	ST2	ST3
#1 UD	1045.4	646.1	205.5
#3 DST	899	589.3	245.1
% Difference	-14.0	-8.8	19.3

Table 3. $\epsilon_{max} - C_L$ gradients for the two plates at different strain gauge locations

To further investigate the reasons for the increased lift coefficient, DIC measurements were examined and are presented in Fig. 14 (a). The DIC measurements indicate that while the tip displacement is reduced (26.9 vs. 26.5mm) for the DST panel, the tip twist is in fact higher when compared to the UD panel (1.6° opposed to 1.2° for the DST and UD panels respectively). An increased twist angle is consistent with the higher lift coefficient created by the DST panel.

Fig. 14 (b) illustrates the validation between the FE model and experimental results obtained for the DST panel. Maximum principal strain measurements are presented for the UD panel with bend twist coupling in Fig. 14 (b) for all three strain gauge locations, comparing the FE model to experimental results produced at the Universities of Bath and Bristol. The results presented were conducted at the wind speed of 20 m/s and a root angle of attack, $\alpha = 3.6^\circ$. In general, it can be noted that the FE model generally overpredicts the strain, and there is generally a good agreement between the measurements conducted at the Universities of Bath and Bristol.



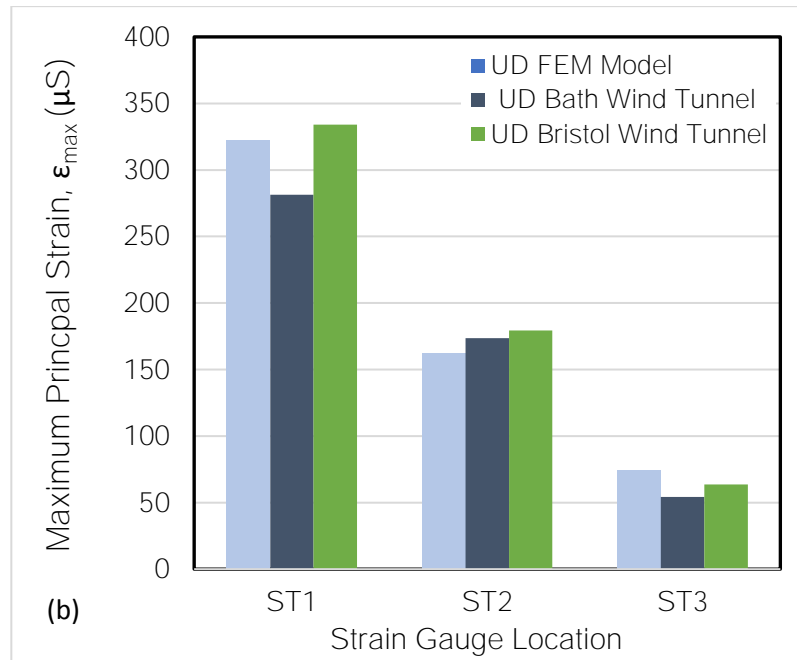


Figure. 14. (a) Contour plots showing displacement for the DST plate (left) and UD with bend-twist coupling (right), conducted at 20m/s, $\alpha = 3.6^\circ$. (b) Maximum principal strain vs. strain gauge location for UD specimen, comparing the FE Model to experimental results obtained at the Universities of Bath and Bristol.

5 DYNAMIC TEST RESULTS

The dynamic behaviour of the plate specimens (without the foam fairings) was subsequently tested. The plates were excited using a frequency sweep from 1 to 300Hz with a drive rod attached 25mm from the root and trailing edge of the plate respectively. The plate was discretised into a grid of forty-five scanning points with nine equidistant span locations and five equidistant chord locations. A Polytec OFV056 laser vibrometer was used to record the velocity at each scanning points during the frequency sweep. A force transducer placed on the drive rod was used to record the force input. The average of three frequency response functions for each scanned point was processed using LMS Test.Lab Modal Analysis software to identify the natural frequencies, damping ratios and mode shapes of each plate specimen.

The test resonance frequencies are compared to the FEM analysis natural frequency predictions in Table 4 for the two straight-fibre (UoB) specimens and the CTS specimen. The modal assurance criterion (MAC) [13] is used to compare the test and FEM predicted mode shapes for the first 6 modes. The MAC for the three UoB specimens is plotted in Fig. 16. There is a good correlation between the dynamic test and analysis results, indicating that the FEM model accurately captures the wing dynamic behaviours. The first 6 modes of the CTS plate are illustrated in Fig. 17, showing the interaction between bending and torsion deflections, characteristic of plates with bend-twist coupling.

(a) Optimised straight fibre (UoB) specimen				(b) the CTS specimen				(c) Straight fibre (UoB) specimen without bend-twist coupling			
Mode #	Test (Hz)	FEM (Hz)	Error (%)	Mode #	Test (Hz)	FEM (Hz)	Error (%)	Mode #	Test (Hz)	FEM (Hz)	Error (%)
1	7.3	7.8	7.6	1	7.4	8.0	7.8	1	8.3	8.9	6.7
2	40.7	38.9	-4.4	2	39.5	39.4	-0.3	2	34.0	30.7	-9.8
3	47.6	49.9	4.8	3	47.8	47.0	-1.5	3	51.9	55.7	7.3
4	121.0	119.6	-1.1	4	125.9	123.5	-1.9	4	112.8	103.3	-8.5
5	140.9	143.7	2.0	5	144.8	152.3	5.2	5	144.7	155.7	7.6
6	225.1	222.2	-1.3	6	242.5	232.1	-4.3	6	216.1	208.0	-3.8

Table 4. Comparison of the analysis and test resonance frequencies for the 3 UoB specimens

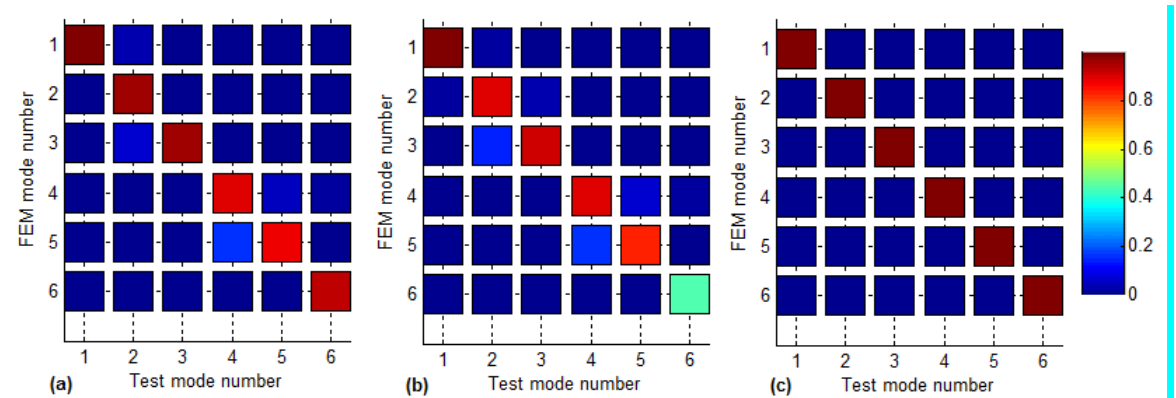


Figure 16. Plot of the MAC for the 3 UoB specimens: (a) the optimised straight fibre (UoB) specimen; (b) the CTS specimen; (c) the straight fibre (UoB) specimen without bend-twist coupling

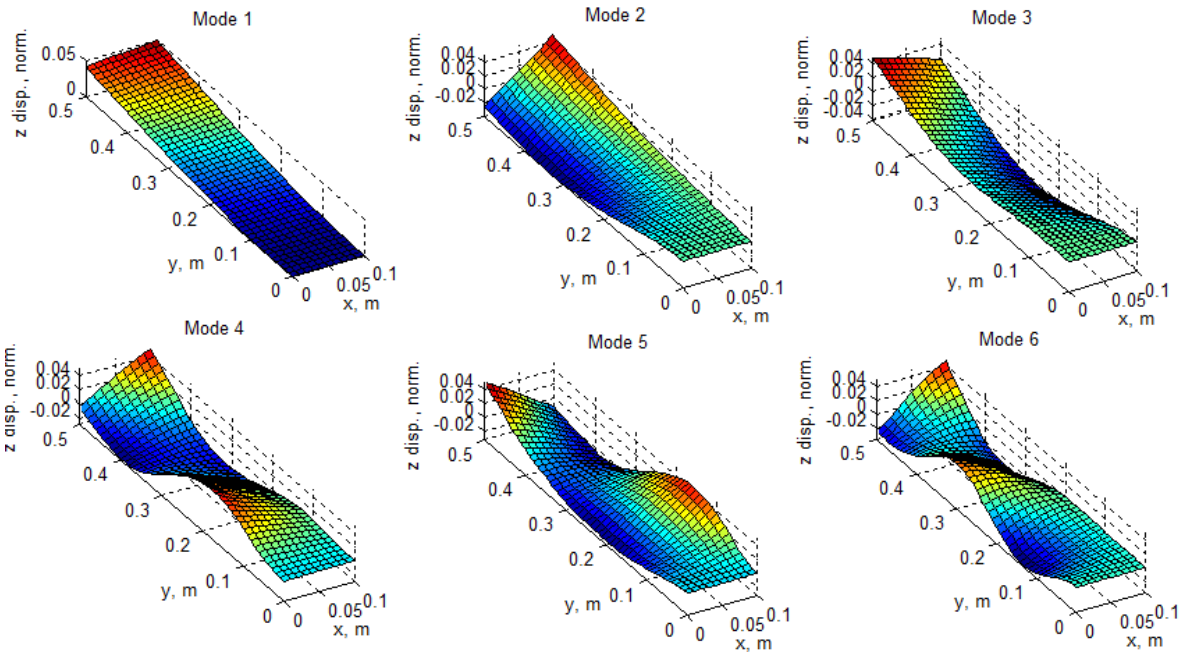


Figure 17. First 6 mode shapes of the CTS specimen, as predicted by the FEM model

6 CONCLUSIONS

A numerical and experimental investigation was undertaken to study the design, manufacture and test of several wind tunnel wings constructed using composite tow-steering methodologies, based upon a configuration of a flat plate with foam aerofoil surfaces. The tow-steered composite layers for the wings were manufactured using two different techniques: Continuous Tow-Shearing and Discrete Stiffness Tailoring. Uni-directional lay-ups were also considered.

Finite Element models of the wings were optimised in order to determine the tow-steered composite layer orientations in order to reduce the maximum strains due to “manoeuvre” and “gust” loads (at 20 m/s). A similar approach was used for the uni-directional lay-up. A series of static and dynamic, wind on/off tunnel tests were performed to validate the numerical modelling capability and to illustrate the capabilities of tow-steering technologies. The results showed that there was a good agreement between the numerical predictions and the test behavior, and that it was possible to use tow-steered composite structures to achieve improved aeroelastic behavior.

7 REFERENCES

- [1] Weisshaar TA. Aeroelastic tailoring of forward swept composite wings, *21st Structures, Structural Dynamics, and Materials Conference*. American Institute of Aeronautics and Astronautics, 1980.
- [2] Shirk MH, Hertz TJ, Weisshaar TA. Aeroelastic tailoring - Theory, practice, and promise, *Journal of Aircraft* 1986;23(1):6-18.
- [3] Eastep FE, Tischler VA, Venkayya VB, Khot NS. Aeroelastic Tailoring of Composite Structures, *Journal of Aircraft* 1999;36(6):1041-7.
- [4] Kim BC, Potter KD, Weaver PM. Continuous tow shearing for manufacturing variable angle tow composites. *Composites Part A* 2012;43:1347-56.
- [5] Kim BC, Weaver PM, Potter K. Manufacturing characteristics of the continuous tow shearing method for manufacturing of variable angle tow composites. *Composites Part A* 2014;61:141-51.
- [6] Kim BC, Potter K, Weaver PM. Multi-tow shearing mechanism for high-speed manufacturing of variable angle tow composites, *15th European Conference on Composite Materials*, 2012.
- [7] Zypeloudis E, Potter K, Weaver PM, Kim BC. Effect of material characteristics on the layup quality of the continuous multi-tow shearing process, *17th European Conference on Composite Materials*, 2016.
- [8] Dodwell TJ, Butler R, Rhead AT. Optimum Fiber Steering of Composite Plates for Buckling and Manufacturability. *AIAA Journal* 2016;54(3):1139-42.
- [9] Stodieck O, Cooper JE, Weaver PM, Kealy P. Improved aeroelastic tailoring using tow-steered composites. *Composite Structures* 2013;106:703-15.
- [10] Stodieck O, Cooper JE, Weaver PM. Optimization of tow-steered composite wing laminates for aeroelastic tailoring. *AIAA Journal* 2015;53:2203-15.
- [11] Stodieck O, Cooper JE, Weaver PM, Kealy P. Aeroelastic Tailoring of a Representative Wing Box Using Tow-Steered Composites to appear in *Journal of Aircraft*. Accepted 17th Oct 2016.
- [12] Stodieck O, Cooper JE, Weaver PM. On the Interpretation of Bending-Torsion Coupling for Swept, Non-Homogenous Wings. *Journal of Aircraft* 2015;54(4):892-9.
- [13] Allemang, R. J., The modal assurance criterion—twenty years of use and abuse. *Sound and vibration* 37.8 (2003): 14-23.

COPYRIGHT STATEMENT

The authors confirm that they, and/or their company or organization, hold copyright on all of the original material included in this paper. The authors also confirm that they have obtained permission, from the copyright holder of any third party material included in this paper, to publish it as part of their paper. The authors confirm that they give permission, or have obtained permission from the copyright holder of this paper, for the publication and distribution of this paper as part of the IFASD-2017 proceedings or as individual off-prints from the proceedings.